Applied Catalysis B: Environmental 256 (2019) 117876

Contents lists available at ScienceDirect

Applied Catalysis B: Environmental

journal homepage: www.elsevier.com/locate/apcatb

Efficient degradation of chloramphenicol by zero-valent iron microspheres and new insights in mechanisms

Jie Yu[a], Xiaoli Hou[a], Xiantao Hu[b], Hong Yuan[a,*], Jingyu Wang[b,*], Chuncheng Chen[c]

[a] Key Laboratory of Pesticide & Chemical Biology of Ministry of Education, College of Chemistry, Central China Normal University, Wuhan, 430079, PR China
[b] Key Laboratory of Materials Chemistry for Energy Conversion and Storage (Ministry of Education), Hubei Key Laboratory of Material Chemistry and Service Failure, School of Chemistry and Chemical Engineering, Huazhong University of Science and Technology, Wuhan, 430074, PR China
[c] Key Laboratory of Photochemistry, CAS Research/Education Center for Excellence in Molecular Sciences, Institute of Chemistry, Chinese Academy of Sciences, Beijing, 100190, PR China

ARTICLE INFO

Keywords:
Zero-valence iron microspheres
Chloramphenicol degradation
Mechanism
Reductive and oxidative transformations

ABSTRACT

Chloramphenicol (CAP) has been extensively used in the broad-spectrum antibiotic therapy so that its excessive emission has brought about serious contamination in aquatic environments. It is of great concern to find an efficient removal method and understand the transformation pathways. In this study, we developed the zero-valence iron based catalytic technique by synthesizing regular zero-valence iron microspheres (ZVI MPs), which could completely remove the CAP pollutant (20 mg L^{-1}) within 15 min. When the CAP concentration increased to 50 mg L^{-1}, the removal efficiency achieved to 95.5% after 15 min of reaction. The chemical evolutions of iron species on the catalyst surface and changes in components of the solution demonstrated the activation of molecular oxygen and hydrogen ion by ZVI MPs. The generation of $^{\cdot}OH$ and $^{\cdot}H$ radicals as well as their contributions to CAP degradation were confirmed by electron spin resonance and trapping experiments during the reaction. Further experiments including the intermediates identification revealed a possible degradation pathway. To the best of our knowledge, the mechanism of CAP degradation by ZVI was proposed for the first time involving both reductive and oxidative transformations with a prerequisite of efficient reductive dechlorination. The complete dechlorination of CAP molecules was confirmed by the detection of inorganic Cl^{-} concentration (0.124 mmol L^{-1} after reaction), which generally lowered the toxicity of the products. These findings not only provided an efficient and economic zero-valent iron technique for eliminating the antibiotic pollutants in water, but also made important contributions to better understand the removal mechanism.

1. Introduction

The extensive use of antibiotics in the treatment of bacterial infections has brought about serious contamination in aquatic environments including surface water and groundwater. Nowadays increasing attention has been given to the efficient removal of such compounds because of their biological toxicity threatening the aquatic organisms and human health [1,2]. Chloramphenicol (CAP) is a kind of broad-spectrum antibiotic drug against several groups of bacteria and microorganisms [3]. The ingestion of water contaminated with CAP may induce detrimental effects such as development of antibiotic resistant bacteria and depression of medullary hematopoiesis function [4]. Considering the inefficiency in removing CAP by conventional wastewater treatment plants, the complete elimination of these antibiotic compounds from water is of great concern.

Many methods for CAP removal have been reported, including physical, biological and chemical treatments. Physical adsorption by porous materials is a nondestructive process which simply accumulated the pollutants on the adsorbents and needed further treatment [5,6]. The antibiotic compounds are generally resistant to destruction by biological treatment in a long time due to their complex and recalcitrant structure. The chemical degradation as one of the most effective techniques is achieved by oxidation or reduction reactions. The oxidative pathways, especially for the advanced oxidation processes (AOPs) are frequently used for organic pollutants removal, which employed the high oxidizing species like reactive hydroxyl and sulfate radicals. The typical reductive pathway may proceed with the generation of hydrogen radical. The chemical degradation of CAP is known to be more difficult than many other types of organic pollutants because it involves the reductive dechlorination and oxidative mineralization. It is of great significance to develop effective methods meeting these requirements, and understand the CAP removal pathways in the aquatic

* Corresponding authors.
E-mail addresses: yuanhong@mail.ccnu.edu.cn (H. Yuan), wangjingyu@hust.edu.cn (J. Wang).

https://doi.org/10.1016/j.apcatb.2019.117876
Received 15 February 2019; Received in revised form 12 June 2019; Accepted 17 June 2019
Available online 18 June 2019
0926-3373/

environment.

Zero-valent iron (ZVI) particles have been considered as effective electron donors capable of rapidly reducing a wide range of organic pollutants due to the advantages of low cost, environmental harmlessness, and low redox potential [7–10]. In particular, ZVI could activate molecular oxygen to generate reactive oxygen species (ROS), and then initiate the oxidative transformation of organic compounds [11–14]. For instance, Waite et al. [15] presented the oxidative degradation of mercapto-containing herbicides by ZVI/air system. Tan et al. [16] proposed the radical generation and evolution in ZVI-mediated oxidative degradation of CAP. It has been reported that the degradation of halogen-binding-based pollutants mostly depended on the reductive dehalogenation efficiency [17–19]. Some groups found that the ZVI could mediate the reductive reactions that were responsible for the pollutant removal from the aqueous solution [20,21]. Zhang [7] and Xu et al. [22] reported that the dechlorination and nitro group reduction were the potential reduction routine of CAP by nanoscale ZVI. Most recently, Donadelli et al. [23] proposed that the removal pathways of ZVI-based system involved both reductive and oxidative transformations, which might be varied in terms of different organic compounds and reaction conditions. This interesting discovery inspired us to design a ZVI-based system to produce reduction and oxidation radicals that contributed to the reductive dechlorination and advanced oxidation of CAP. Although there are numbers of reports on pollutant removal by ZVI-based technology, most of them only partially focus on the oxidative or reductive removal process, and the mechanism of CAP degradation pathways is still unclear so far.

In comparison to commercial ZVI, nano-sized ZVI particles have been reported to exhibit a high catalytic activity owing to the improved dispersibility and specific surface area. However, ZVI nanoparticles are easily agglomerated during the reaction with H_2O and O_2 and suffer from serious corrosion to the formation of passivation layer containing the iron oxides and hydroxides. These changes substantially decreased the catalytic activity and utilization efficiency of ZVI nanoparticles [24,25]. In this work, we synthesized regular zero-valence iron microspheres (ZVI MPs) via a liquid-phase reduction method. The as-obtained ZVI MPs, with the particle size between commercial bulk and nanoscale, provided an effective way to combine the advantages of excellent catalytic activity and moderate structural stability towards CAP degradation. Furthermore, the kinetics and reactive species were investigated to evaluate the contributions of reductive and oxidative transformations. The changes in the structure of ZVI MPs as well as the reduction and oxidation products were also analyzed to present the mechanisms of CAP degradation.

2. Experimental

2.1. Chemicals

Sodium borohydride ($NaBH_4$, 96%), Ferrous chloride tetrahydrate ($FeCl_2{\cdot}4H_2O$), ferrous sulfate heptahydrate ($FeSO_4{\cdot}7H_2O$), Sodium acetate, Hydroxylamine hydrochloride, 1,10-*ortho*-phenanthroline, *Tert*-butyl alcohol, and Ethanol were obtained from National Medicines Corporation Ltd., China, and the above chemical were of analytical grade. Dichloromethane (Chromatography grade), *N*-hexane (Chromatography grade), Silane reagent (chromatography grade), Bipyridine (Analytical Reagent), *P*-hydroxybenzoic acid (Analytical Reagent) and Benzoic acid (Analytical Reagent) were bought from Aladdin Reagent Corporation Ltd. (Shanghai, China). Chloramphenicol (Top grade pure) was purchased from Acros company. Methanol (chromatography grade) was purchased from TEDIA world reagent company. The deionized water (18.2 MΩ cm, a Milli-Q system) was used during all experiments.

2.2. Preparation of zero-valence iron microspheres (ZVI MPs)

The zero-valence iron microspheres were prepared via a liquid-phase reduction method using ethylenediamine as chelating and structure-directing agent. The deionized water was deoxygenated by continuously purging with N_2 gas for 30 min before use. In a typical synthesis, 4.455 g of tetrahydrated ferrous chloride ($FeCl_2{\cdot}4H_2O$) was added into a 1000 mL four-necked flask containing 300 mL distilled water. 4.05 g of ethylenediamine were dissolved in 75 mL of distilled water, and then poured into the four-neck flask. After mixing, the color of the solution changed from light green to dark green, indicating the formation of iron(II)-ethylenediamine complex. Subsequently, 4.455 g of sodium borohydride were dissolved in 75 mL of distilled water and dropped into the above mixture. At this time, the black flocculent precipitate was generated together with the evolution of H_2 gas. After stirring the reaction solution for 1 h, the synthesized ZVI MPs samples were collected by magnet, and then washed with the deionized water and ethanol for three times, finally blow-dried under the protection of N_2 gas. During the whole preparation process, high purity N_2 gas was continuously bubbled into the four-neck flask at a flow rate of 1.0 L min^{-1}. The dried ZVI MPs were kept in a vacuum glove box for further use.

2.3. Characterizations

Scanning electron microscopic (SEM) images were observed on a Rio Scanning electron microscopy (Germany). Transmission electron microscopic (TEM) images were obtained using a JEOL transmission electron microscopy (Japan). X-ray powder diffraction (XRD) pattern were collected with a Rigaku D/MAX-RB X-ray powder diffractometer (Cu Ka radiation, λ = 1.54178 Å). X-ray photoelectron spectroscopy (XPS) was recorded by an X-ray photoelectron spectroscope (15 kV, 10 mA, Thermo, USA).

2.4. CAP removal experiments

In a typical degradation process, 0.02 g of ZVI MPs catalyst was introduced into 20 mL of aqueous solution containing a certain concentration of CAP stock solution varied from 10 to 100 mg L^{-1} in a 50 mL conical flask. The reaction proceeded on a reciprocal shaker at 25 °C and a rotation rate of 500 rpm. During the process, the vessel was open to keep the oxygen concentration under equilibrium condition. The samples were taken at a time interval of five minutes during the reaction, and then filtered through the filter membrane for quantitative analysis. The control experiment was conducted to study the effect of dissolved oxygen on the CAP degradation. The reaction system was deoxygenated by continuously purging with high purity Ar gas for 30 min and then sealed for isolation from air.

The concentration of CAP in the solution was quantified by high performance liquid chromatography (HPLC, LC-20A, Shimadzu, Japan) equipped with a TC-C18 reverse phase column (4.6 × 150 mm, 5 μm, Agilent, USA). The mobile phase was composed of acetonitrile and acid aqueous solution (0.1% formic acid) with the volume ratio of 75:25. The gradient profile was obtained at a flow rate of 0.7 mL min^{-1} and an injection volume of 10 μL using the absorbance wavelength of 277 nm. The temperature of column was maintained at 30 °C. The change of total organic carbon (TOC) during degradation process was measured by TOC-VCPH TOC analyzer (Shimadzu, Japan).

2.5. Analytical methods of intermediates and active species

The active species such as hydrogen radical (·H) and hydroxyl radical (·OH) were determined by electron spin resonance (ESR) spectroscopy (Bruker EMX, Billerica, MA). After adding the ZVI MPs catalyst into 40 mL of 10 mg L^{-1} CAP solution, the 0.01 mmol 2,2,6,6-tetramethylpiperidine-1-oxygen free radicals (TEMPO) and 0.005 mmol 5,5-

dimethyl-1-pyrroline-N-Oxide (DMPO) were introduced as ˙H and ˙OH spin trappers, respectively. At given time intervals, 10 μL of mixture were taken out from the reaction system to determine the concentration of ˙H or ˙OH. For determination of the ˙OH concentration, benzoic acid method was described as follows [12]. 0.02 g of ZVI MPs was added into 20 mL of 20 mg L^{-1} benzoic acid solution. At given time intervals, the amount of hydroxybenzoic acid was detected by HLPC using the same reverse phase column and detector as the detection of CAP concentration. The mobile phase was composed of acetonitrile and 0.2% acetic acid with the volume ratio of 30:70. The gradient profile was obtained at a flow rate of 1.0 mL min^{-1} and an injection volume of 10 μL using the absorbance wavelength of 255 nm.

The concentration of H_2O_2 was determined by fluorescence method [26]. The H_2O_2 fluorescent reagent was composed of 10 mg of potassium hydrogen phthalate (KHP), 1.0 mg of horseradish peroxidase (POD) and 2.7 mg of *p*-hydroxyphenylacetic acid (*p*-HPA). The mixture was dissolved to 20 mL of water, and then 0.02 g of ZVI MPs was added to start reaction. At a certain time interval, 2.5 mL of sample was taken out and statically placed for 10 min, and then 1 mL of 1 M NaOH solution was added. The fluorescence intensity was determined at the emission wavelength of 409 nm with an excitation wavelength of 315 nm using a Clary Eclipse fluorescence spectrophotometer (Agilent, USA).

The dechlorination of CAP was monitored by Metrohm 861 type ion chromatograph (IC, Thermo, USA) with a Metrosep A supp4 ion chromatographic column (250 mm × 4.0 mm). The eluent was of 0.8 mmol L^{-1} $NaHCO_3$ and 4.5 mmol L^{-1} Na_2CO_3 solution at a flow rate of 1.0 mL min^{-1}. The organic intermediates were determined by gas chromatography-mass spectrometer (GC–MS, Thermo Trace 1300-ISQ, USA) equipped with a HP-5MS capillary column (30 m × 0.25 mm × 0.25 μm) and liquid chromatography-mass spectrometer (LC–MS/MS, Thermo TSQ Quantum Access MAX, USA) equipped with a Hypersil GOLD C18 packed column (150 × 2.1 mm, 300 Å). The sample in aqueous phase was extracted with dichloromethane and then collected by drying and dispersing into acetone for GC–MS measurement. Standard analysis conditions were injection volume of 1 μL, injector temperature of 240 °C, detector temperature of 260 °C, and column temperature program of increasing from 50 °C (hold 3 min) to 260 °C (hold 20 min) at a rate of 5 °C min^{-1}. The sample in aqueous phase was extracted with dichloromethane and then collected by drying and dispersing into methanol for LC–MS measurement. Standard analysis conditions were injection volume of 5 μL and scanning range of m/z = 60–350. The eluent was composed of acetonitrile and acid aqueous solution (0.1% formic acid) with the volume ratio of 75:25 at a flow rate of 0.2 mL min^{-1}.

3. Results and discussion

3.1. Structural analysis

The morphology of the as-prepared zero-valent iron particles was analyzed by SEM and TEM observations. Fig. 1a displayed a sphere structure with a diameter of 900–1000 nm. The ZVI particles possessed regularly spherical appearance, and the surface was relatively smooth (Fig. 1b–c). It was observed that these microspheres were inclined to form a chain-like structure due to their magnetic interactions [27]. In the absence of ethylenediamine, the color of the reaction solution rapidly changed to black as a result of fast reduction. The product displayed a wire-like nanostructure that was composed of much smaller nanospheres (Fig. S1). It was reported that the reduction rate of iron ions by sodium borohydride influenced the morphology and crystallinity of ZVI. Zhang et al. [28] found that decreasing the adding rate of sodium borohydride could slow down the reduction rate to produce chain-like ZVI with the sphere size increasing from 50–100 to 50–200 nm and lower crystallinity. In this work, the reduction process apparently occurred much slower by the chelation with ethylenediamine, resulting in the formation of larger ZVI microspheres. As shown in Fig. 1d, there was a broad peak at $2\theta = 44.7°$ in the XRD pattern, indicating the amorphous structure of pure zero-valent iron (JCPDS No. 3-1050).

3.2. Efficiency and kinetic analysis of CAP removal

The amount of ZVI MPs had great impact on the CAP removal efficiency. The CAP concentration was detected to be constant in the absence of ZVI MPs during 30 min of duration time. As shown in Fig. 2a, the degradation efficiency obviously increased with the dosage of ZVI MPs from 0.01 to 0.04 g. The great improvement of the catalytic efficiency could be attributed to the catalytic reaction occurring on the surface of ZVI MPs and the increased available surface sites for CAP adsorption and reaction [7]. On the other hand, the concentration of CAP also had important influence on the removal efficiency. At low concentration (below 50 mg L^{-1}), almost complete removal of CAP could be achieved within 15 min of reaction with 0.05 g of ZVI MPs (Fig. 2b). If increasing the CAP concentration to 100 mg L^{-1}, the CAP pollutant could not be completely removed after 30 min together with a great drop in the degradation rate. It is noted that the condition of 0.04 g ZVI MPs and 20 mg L^{-1} CAP in Fig. 2a presented the same ratio of catalyst to CAP as the condition of 0.02 g ZVI MPs and 10 mg L^{-1} CAP in Fig. 2b. By comparison, the CAP degradation rate showed great difference, i.e. much higher rate in the case of higher initial concentration of catalyst and CAP. Some groups also observed the higher degradation rate of pollutant at higher initial concentration of catalyst even the ratio of catalyst to pollutant was similar [10,29]. The results suggested that the reaction rate constant was influenced by the initial concentration of catalyst and CAP. It can be deduced that the whole reaction is not a strict characteristic of first-order kinetic model. There might be several other factors influencing the reaction rate, such as the reactant/product transport efficiency, the available active sites on ZVI surface for adsorption and reaction, the collision frequency of reactants and so on. Besides, the formation of the passivation layer covering the catalyst varied under different conditions [30]. This indicated a complicated reaction mechanism of CAP degradation over ZVI MP catalysts.

3.3. Changes in the composition of catalytic system

The pH value of the system increased with the reaction time (Fig. 3a), which was in accordance with the reported results of ZVI catalysts [30–33]. The rapid change in pH value at the initial reaction stage suggested the H^+ reduction in the presence of ZVI, accompanying by the oxidation of catalysts to the formation of Fe^{II} and Fe^{III} species. The rate of pH increase was slowed down at extended reaction time, due to the growth of iron oxides or hydroxides on ZVI surface inhibiting the further reaction with protons. The increased degradation efficiency under higher acidic condition as shown in Fig. 3b was presumably due to the production of abundant hydrogen for reductive reaction, which confirmed the consumption of H^+ during CAP degradation.

To study the role of ZVI MP catalysts in CAP degradation, the structure and chemical composition before and after reaction were compared. It was observed that the surface of ZVI microspheres after reaction was no longer smooth, but became rough with many nanoparticles covering (Fig. 4a–c). The XRD pattern in Fig. 4d indicated that the zero-valent iron was partly oxidized to Fe_2O_3 (25-1402 Magnetite-Q, syn Fe_2O_3) during reaction. Fig. 5 presented the high-resolution XPS spectra of Fe 2p and O 1s. The deconvoluted Fe 2p spectrum revealed that the newly prepared ZVI MPs contained more than one type of Fe species (Fig. 5a). Two main peaks at 709.6 and 722.8 eV could be ascribed to the binding energy of Fe 2p3/2 and Fe 2p1/2 in iron oxide state. Two distinct shoulder peaks at 705.8 and 718.8 eV were the characteristic signals of Fe^0 species. According to the peak deconvolution, the peak at 709.6 eV could be divided to 709.2 and 711.0 eV, which were assigned to Fe^{II} and Fe^{III} species [34–36]. Since the XRD

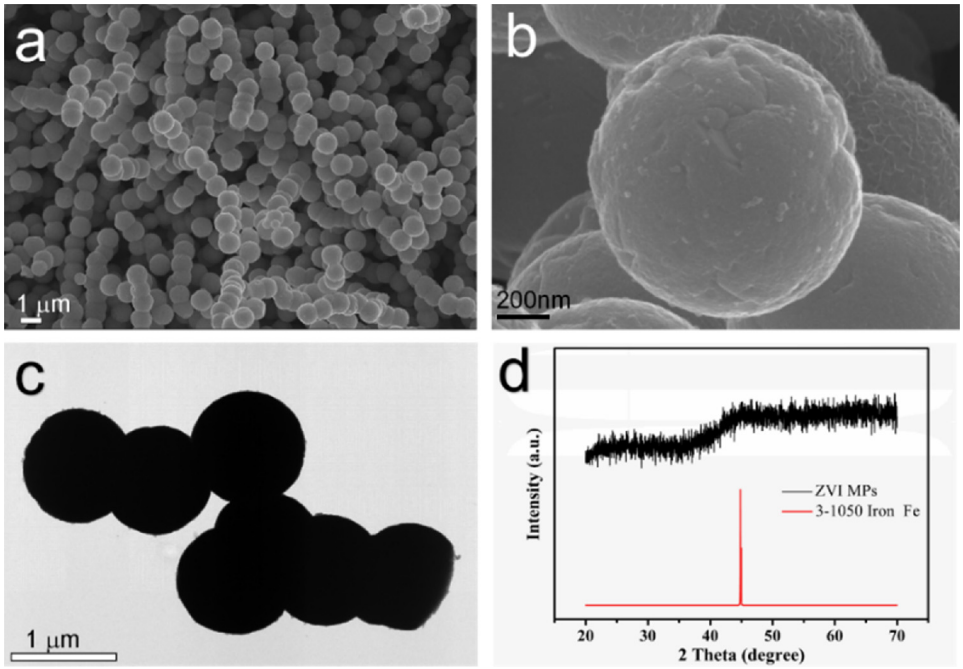

Fig. 1. (a–b) SEM image, (c) TEM image, and (d) XRD pattern of ZVI MPs.

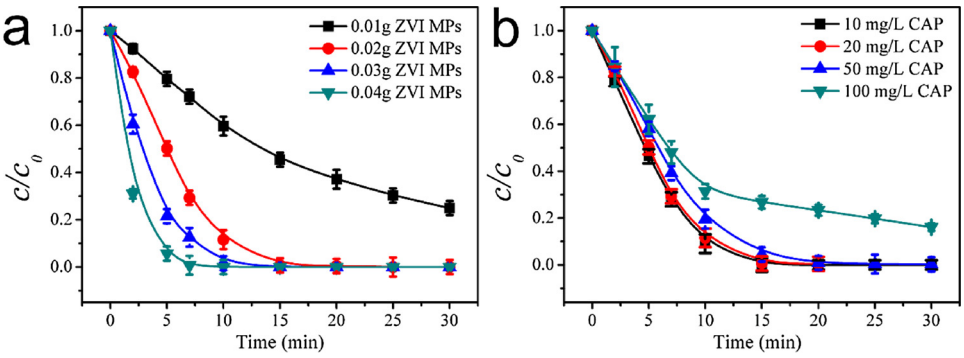

Fig. 2. Effects of ZVI MPs dosage and initial CAP concentration on the removal efficiency of CAP. (a) Time-dependent changes with varied ZVI MPs concentration. The initial CAP concentration is 20 mg L^{-1}. (b) Time-dependent changes with varied CAP concentration. The ZVI MPs dosage is 0.02 g.

pattern of ZVI MPs in Fig. 1c did not show other Fe species but only amorphous Fe^0, the surface of ZVI MPs might contain a part of iron oxides. After the reaction, the intensity of Fe^0 signals greatly weakened, indicating that the activation of molecular oxygen by Fe^0 produced iron oxides on the surface of ZVI MPs [37]. The proportions of these Fe species before and after the reaction were calculated by the peak area, and compared in Table 1. After the reaction, the Fe^0 content was decreased from 14.1% to 10.9%, and the Fe^{II} content was decreased from 40.5% to 29.1%. On the contrary, the Fe^{III} content was increased from 45.4% to 60.0%. The above results indicated that the Fe^0 and Fe^{II} species were converted to Fe^{III} species during the reaction. The O 1s spectrum could be deconvoluted into three peaks at 528.8, 530.2 and

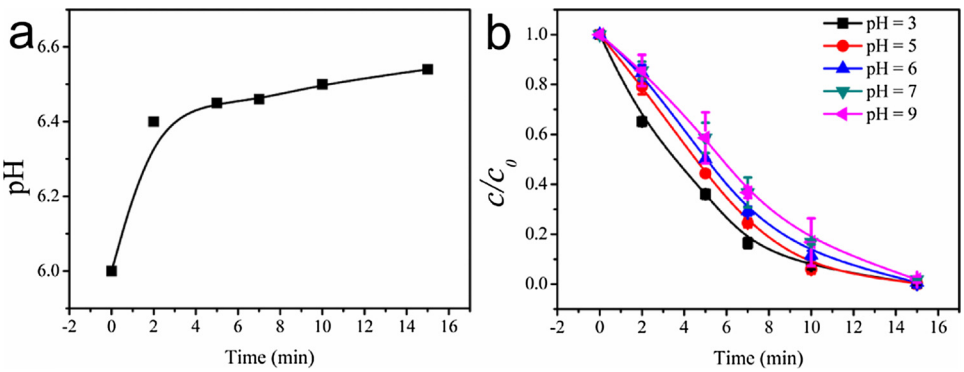

Fig. 3. (a) Changes in pH value during CAP degradation over ZVI MPs; (b) effect of initial pH value on the removal efficiency of CAP. Experiment conditions: 0.02 g ZVI MPs, 20 mg L^{-1} CAP solution.

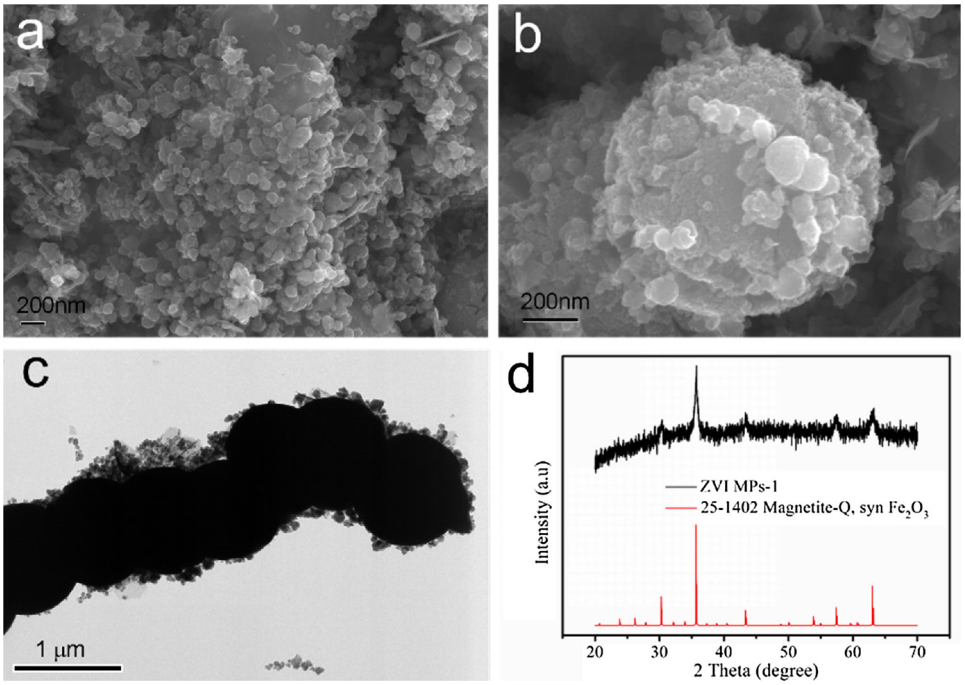

Fig. 4. (a–b) SEM image, (c) TEM image, and (d) XRD pattern of ZVI MPs after reaction.

531.5 eV, corresponding to Fe_2O_3, Fe−OH and adsorbed water [38,39]. The intensity of Fe−OH signal obviously decreased during the reaction, while that of Fe_2O_3 signal increased accordingly (Fig. 5b). Combined with the changes in surface morphology and crystal phase, it could be deduced that most of the Fe species on the surface of ZVI MPs were converted to iron oxide nanoparticles. The changes in the concentration of Fe^{2+} and Fe^{3+} ions in the solution were monitored during reaction. As shown in Fig. S2, the total concentration of iron ions gradually increased with the reaction, which came from the increase in Fe^{2+} concentration because the concentration of Fe^{3+} ions was extremely low and almost kept constant. As a result, the evolution of Fe species on the surface of ZVI MPs could be explained by the dissolution of Fe^{II} species to the solution, and the precipitation of Fe^{3+} ions on the ZVI MPs surface from the solution during reaction.

3.4. Active species to CAP degradation by ZVI MPs

To reveal the mechanism of CAP degradation by ZVI MPs, we conducted a series of controlled experiments with addition of scavengers. The *tert*-butyl alcohol (TBA) and benzoquinone (BQ) were introduced to the reaction system for trapping $^{\cdot}OH$ and $O_2^{-\cdot}$ respectively (Fig. 6a). It was observed that the degradation rate of CAP was slightly affected in the presence of BQ, which revealed the little contribution of $O_2^{-\cdot}$ in the ZVI MPs system. Trapping test with TBA caused a dramatic decrease in the removal efficiency from 100% to 60% in 15 min, indicating that the $^{\cdot}OH$ radicals were the main reactive oxygen species contributing to the degradation of CAP. In the ZVI MPs catalytic system, the $^{\cdot}OH$ radicals were generated by the reaction of Fe^{II} with H_2O_2. Since the concentration of Fe^{2+} ions in the solution gradually increased with the reaction, the role of Fe^{2+} ions in CAP degradation could be studied by adding the complexing agent. The introduction of excess bipyridine (BPY) to the solution could produce iron(II) complexes in the system, and thus inhibit the reaction with H_2O_2 to generate Fe^{3+} and $^{\cdot}OH$ [31,40]. However, the degradation rate of CAP was not affected by BPY addition (Fig. 6b). The results were in accordance with the extremely

Table 1
The ratio of the peak area of the valence state Fe and the total peak area before and after the ZVI MPs reaction.

ZVI MPs	Fe^0/Fe_{total}	Fe^{II}/Fe_{total}	Fe^{III}/Fe_{total}	$Fe-OH/O_{total}$	Fe_xO_y/O_{total}
Fresh	14.1%	40.5%	45.4%	58.3%	36.8%
Used	10.9%	29.1%	60.0%	42.1%	40.4%

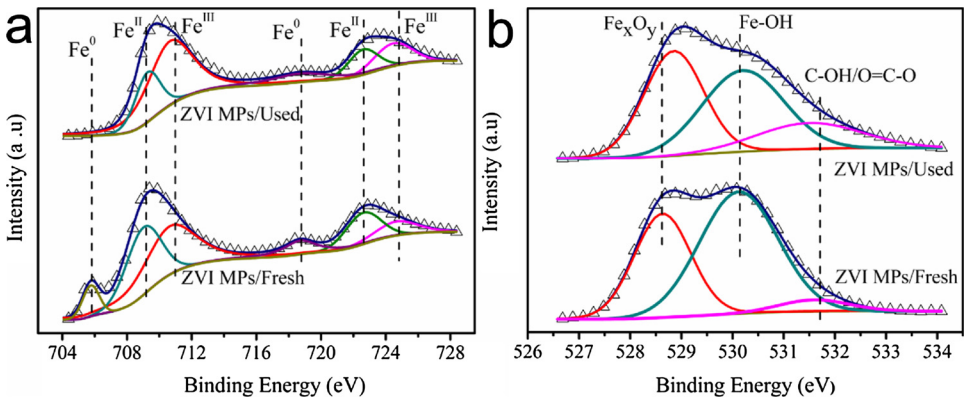

Fig. 5. XPS spectrum before and after ZVI MPs reaction: (a) Fe 2p, (b) O 1s.

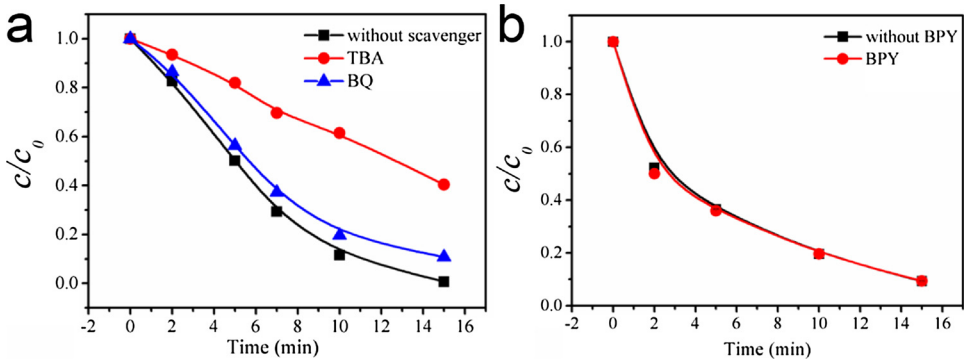

Fig. 6. Comparison of CAP degradation in the presence and in the absence of scavengers. (a) *tert*-Butyl alcohol (TBA) for ˙OH and benzoquinone (BQ) for O_2^{-}˙; (b) bipyridine (BPY) for Fe^{2+}.

low concentration of Fe^{3+} in the solution that produced by the reaction (Fig. S2). Combined with the changes in Fe species on ZVI MPs surface (Fig. 5), it could be deduced that the ˙OH radicals might originate from the Fe^{II} species on the ZVI MPs surface rather than the Fe^{2+} ions in the solution.

ESR measurements were conducted to further confirm the role of ˙OH radicals in CAP degradation. The 1:2:2:1 characteristic quartet of ˙OH could be observed on the ESR pattern of ZVI MPs system without addition of CAP pollutant (Fig. 7a). However, the signals almost disappeared in the ZVI MPs/CAP system (Fig. 7b), indicating that ˙OH was produced in the system, and then immediately reacted with the contaminants. The changes in the concentration of ˙OH and H_2O_2 were also monitored in the ZVI MPs system without CAP, as shown in Fig. 7c–d. The amount of ˙OH gradually increased, and the concentration could reach 3 μmol L^{-1} at 15 min, while the concentration of H_2O_2 increased at the beginning, and then rapidly decreased. In the absence of O_2 gas, there was no H_2O_2 and ˙OH that generated from the system. Combined with the above results, the oxidation reactions occurred on the ZVI MPs surface could be proposed as follows (Eqs. (1) and (2)).

$$Fe^0 + O_2 + 2H^+ \rightarrow Fe^{II} + H_2O_2 \quad (1)$$

$$Fe^{II} + H_2O_2 \rightarrow Fe^{III} + {}^{\cdot}OH + OH^- \quad (2)$$

First, the molecular oxygen was activated by Fe^0 to the formation of H_2O_2. Then the generated H_2O_2 reacted with Fe^{II} species on the ZVI MPs surface to produce ˙OH. The ˙OH radicals were highly reactive to induced the degradation of CAP.

It should be noted that the elimination of ˙OH radicals by scavenger did not completely inhibit the degradation of CAP. The degradation efficiency of CAP still reached 60% in the presence of ˙OH scavenger, indicating that the reductive species also made contributions to CAP removal besides reactive oxygen species. Due to more negative potential of Fe^0/Fe^{2+} (−0.44 V vs NHE) than that of ˙H/H^+ (0 V vs NHE), the H^+ ions that adsorbed on the ZVI MPs surface could trap the electrons to be reduced to ˙H together with the oxidation of Fe^0 to Fe^{II} (Eq. (3)) [13]. When TEMPO was added to the system, TEMPO reacted

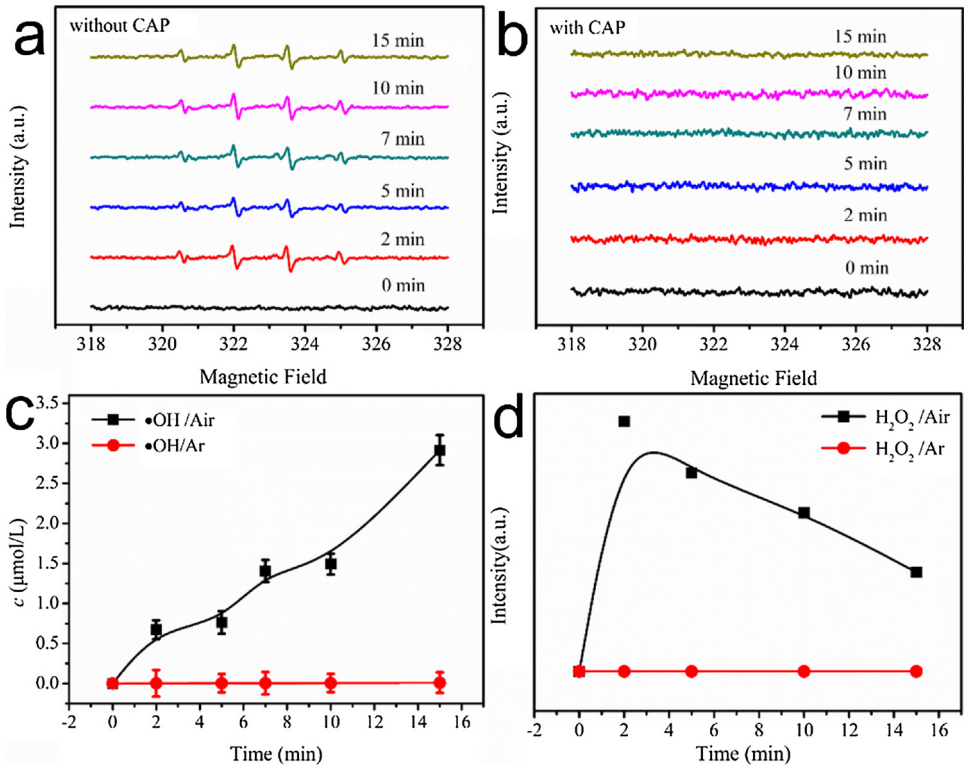

Fig. 7. DMPO spin-trapping ESR spectra in the ZVI MPs system (a) without CAP and (b) with CAP. Determination of the concentration of (c) ˙OH and (d) H_2O_2 in the ZVI MPs system without CAP under different gas environment.

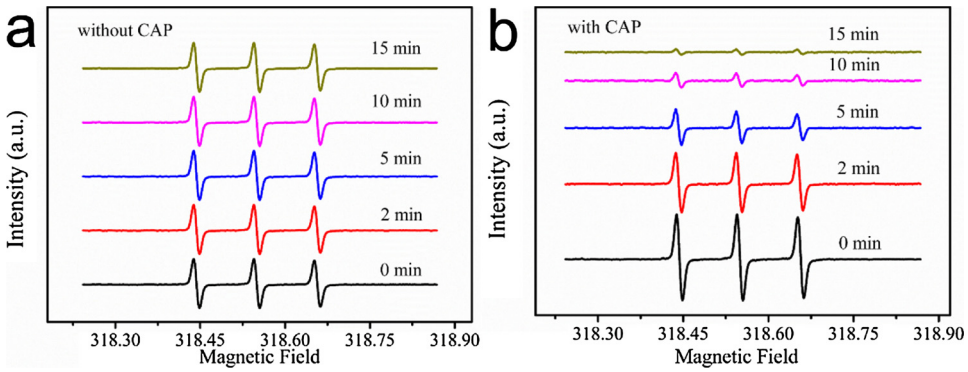

Fig. 8. TEMPO spin-trapping ESR spectra in the ZVI MPs system (a) without CAP and (b) with CAP.

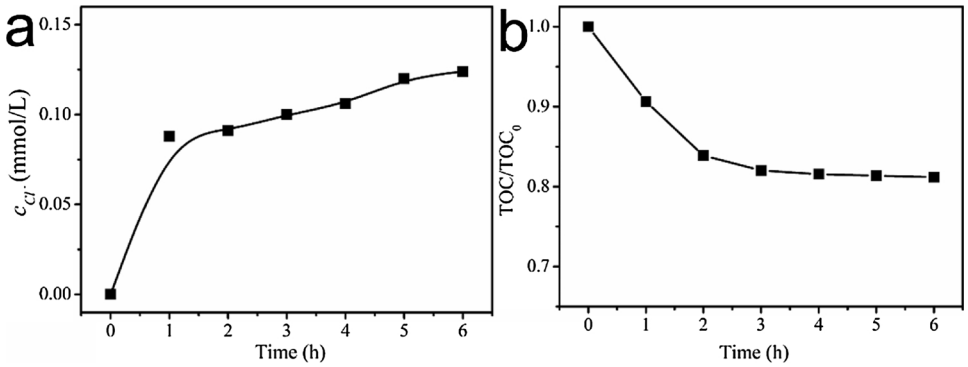

Fig. 9. Changes in (a) Cl^- concentration and (b) TOC during the CAP degradation by ZVI MPs catalysts.

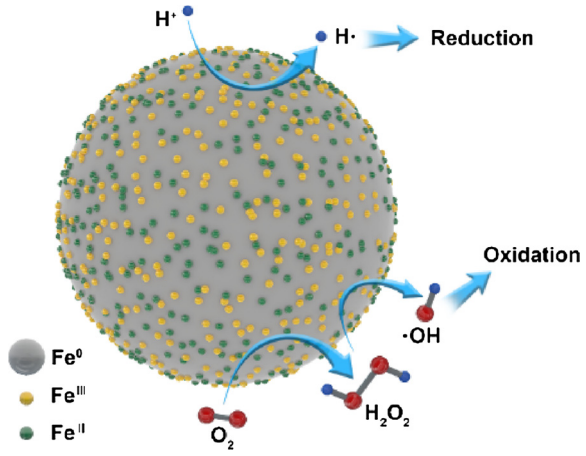

Fig. 10. Mechanism of active species production during CAP degradation by ZVI MPs.

quickly with ˙H to produce TEMPO/˙H signals in the ESR spectra. The typical signals of TEMPO/˙H in Fig. 8a confirmed that the ˙H could be produced in the ZVI MPs system. After the addition of CAP pollutants, the intensity of TEMPO/˙H signals gradually weakened as the reaction proceeded (Fig. 8b), suggesting that the ˙H radicals that produced by ZVI MPs were consumed by CAP during the reaction. That is, the generation of ˙H radicals initiated the reductive degradation of CAP. Meanwhile, the ˙H radicals could also be recombined to produce H_2 (Eq. (4)). The H_2 production was seriously inhibited in the presence of CAP (Fig. S3), which further verified the contribution of ˙H radicals to CAP degradation process. On the other hand, the generated ˙H could be quickly scavenged by dissolved O_2 to produce $^{\cdot}HO_2$ and H_2O_2 (Eqs. (5) and (6)), which would subsequently convert to ˙OH [41,42].

$$Fe^0 + 2H^+ \rightarrow Fe^{II} + 2^{\cdot}H \quad (3)$$

$$^{\cdot}H + {}^{\cdot}H \rightarrow H_2 \quad (4)$$

$$^{\cdot}H + O_2 \rightarrow {}^{\cdot}HO_2 \quad (5)$$

$$^{\cdot}HO_2 + {}^{\cdot}H \rightarrow H_2O_2 \quad (6)$$

Since the ˙H radicals were capable of trapping electrons from the dissolved O_2, their contributions to CAP degradation might include both the direction reduction and the induced oxidation by ROS species. Another controlled experiment was carried out under Ar condition to eliminate the influence of O_2. Interestingly, the complete removal of CAP was achieved within 7 min in Ar atmosphere (Fig. S4). According to a pseudo first-order kinetic model, the rate constant was 2.6 times higher than that in air. As a result, the oxidative degradation of CAP on the ZVI MPs surface was achieved at the sacrifice of reductive degradation. Based on the above discussions, it is well-established that the removal pathways of CAP in the ZVI MPs system involved both oxidative and reductive transformations.

3.5. Determination of degradation intermediates

To illustrate the pathways of CAP degradation, the intermediates by reductive and oxidative transformations were identified by IC, GC–MS and LC–MS techniques. Generally, the dehalogenation of CAP was a crucial step that achieved by the reduction reaction, resulting in the formation of chloride ions (Cl^-) in the solution [7,43]. The changes in the concentration of Cl^- during CAP degradation were monitered by ion chromatography. The concentration of Cl^- in the solution dramatically increased at the initial stage, and then changed slowly at the extended reaction time (Fig. 9a). After reaction for 6 h, the concentration of Cl^- reached 0.124 mmol L^{-1}, which was consistent with the theoretical value, indicating that 100% of the organic chlorine in the CAP molecules were transformed to non-toxic inorganic Cl^- ions. Although the removal efficiency reached 100% within 15 min, the total organic carbon (TOC) could only decrease to 18% of the initial value

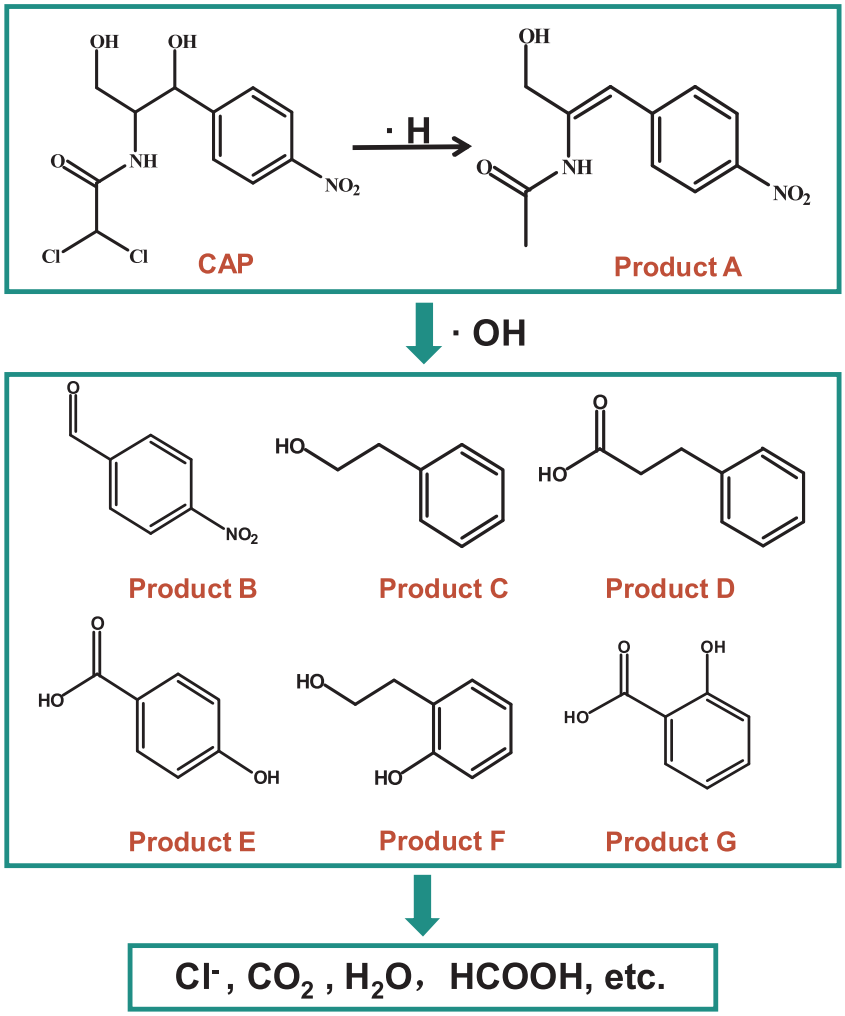

Fig. 11. The possible pathways of CAP degradation.
Product A: *N*-[1-(hydroxymethyl)-2-(4-nitrophenyl)ethenyl]-acetamide, Product B: 4-nitrobenzaldehyde, Product C: phenethyl alcohol, Product D: 3-phenylpropanoic acid, Product E: 4-hydroxybenzoic acid, Product F: 2-hydroxyphenethyl alcohol, Product G: 2-hydroxybenzoic acid.

after reaction for 3 h, and then displayed a slow decrease when the reaction time was extended to 6 h (Fig. 9b), which was in accordance with the literatures on CAP degradation [43,44]. As a result, the TOC removal of CAP pollutants largely depended on the degradation of the side chain groups on the benzene ring; by contrast, further removal would be more difficult, and need longer time to achieve ring opening degradation. Generally, dehalogenation is a straightforward approach for detoxifications of harmful halogenated aromatic compounds [45–47]. Although the degraded products are still aromatics and may possess high toxicity, some of them normally possess lower toxicity in comparison to CAP molecules due to the complete dichlorination.

Based on the results of GC–MS and LC–MS, the possible intermediates were indentified, and listed in Fig. S5 and Table S1. Therefore, the mechanism of active species production as well as the evolution of Fe species on the surface of ZVI MPs catalyst during CAP degradation was proposed in Fig. 10. The zero-valent iron could react with the adsorbed H^+ ions to produce $^{\cdot}H$ radicals, which attacked the CAP molecules to induce the reductive transformation. Meanwhile, the $^{\cdot}H$ radicals would also be oxidized by the dissolved O_2 to yield H_2O_2. On the other hand, the zero-valent iron could also activate the molecular oxygen to the formation of H_2O_2. Accordingly, the Fe^0 on the ZVI MPs surface was oxidized to Fe^{II} species, which were readily to react with H_2O_2 to generate $^{\cdot}OH$ radicals. Thus, the superficial Fe species were partially converted to Fe^{III} species, and existed as Fe_2O_3 nanoparticles covering the ZVI MPs surface after the reaction (Fig. 10). Because of the dual roles of ZVI MPs in producing reduction and oxidation radicals, the CAP pollutants undergo both reductive and oxidative transformations to be degraded to products with low toxicity and some completely mineralized molecules. The CAP degradation pathway in the ZVI MPs catalytic system was illustrated in Fig. 11. Compound A, the product of breaking C—Cl bonds of CAP, was mainly originated from the reductive dechlorination of CAP by $^{\cdot}H$ radicals. Then, the Product A was attacked by $^{\cdot}OH$ radicals to induce the cleavage of the amide group to produce Product B, C and D, which would be further oxidized to Product E-G with much lower toxicity than CAP, and finally were mineralized by $^{\cdot}OH$ to yield small molecules. The concentration of HCOOH in the solution gradually increased with the reaction (Fig. S6), which further verified that the intermediate products such as Product D, E and G contained carboxylic acid groups.

4. Conclusion

In summary, the regular ZVI microspheres with a diameter of 900–1000 nm were successfully synthesized by a liquid-phase reduction method. The as-obtained ZVI MPs exhibited excellent catalytic activity and moderate stability towards degradation of 20 mg L^{-1} CAP solution, achieving the removal efficiency of 100% within 15 min. When the CAP concentration increased to 50 mg L^{-1}, the removal efficiency achieved to 95.5% after 15 min of reaction in the presence of 1.0 g L^{-1} ZVI catalyst. The molecular oxygen and hydrogen ions could be activated by

ZVI MPs, resulting in the production of reactive oxygen species and ˙H radicals. Accordingly, most of the Fe^0 species on the surface of ZVI MPs were converted to Fe^{III} species that existed as iron oxide nanoparticles covering the ZVI surface. The main contributions of ˙OH and ˙H radicals to CAP degradation were confirmed by electron spin resonance and trapping experiments during the reaction. Based on the identification of intermediates, the mechanism of CAP degradation by ZVI was proposed. The CAP pollutants underwent reductive dechlorination at the first step, and then were further oxidized to the degraded products. In comparison to CAP molecules, the products normally possess lower toxicity due to the complete dichlorination, which was evidenced by the production of 0.124 mmol L^{-1} Cl^- ions after the reaction. Overall, the efforts that made in this work provided better understanding for the transformation pathways of CAP, which could direct the development of more effective methods for elimination of such antibiotic compounds in the environment.

Conflict of interest

None.

Acknowledgments

This work was financially supported by the National Natural Science Foundation of China (Grant Nos. 21277055, 21771070), the 111 Project B17019 and the Fundamental Research Funds for the Central Universities (2018KFYYXJJ120, 2019kfyRCPY104).

Appendix A. Supplementary data

Supplementary material related to this article can be found, in the online version, at doi:https://doi.org/10.1016/j.apcatb.2019.117876.

References

[1] K. Kümmerer, Chemosphere 75 (2009) 417–434.
[2] V. Homem, L. Santos, J. Environ. Manage. 92 (2011) 2304–2347.
[3] H.J. Balbi, Pediatr. Rev. 25 (2004) 284–288.
[4] B.E. Wiholm, J.P. Kelly, D. Kaufman, I. Surapol, M. Levy, T. Anderson, S. Shapiro, Br. Med. J. 316 (1998) 666.
[5] X.D. Zhao, H.F. Zhao, W.J. Dai, Y.N. Wei, Y.Y. Wang, Y.Z. Zhang, Z. Zhang, L.F. Zhi, H.L. Huang, Z.Q. Gao, J. Colloid Interface Sci. 526 (2018) 28–34.
[6] F. Fan, B. Wang, S.H. Yuan, X.H. Wu, J. Chen, L.L. Wang, Bioresour. Technol. 101 (2010) 7661–7664.
[7] S.Q. Xia, Z.L. Gu, Z.Q. Zhang, J. Zhang, S.W. Hermanowicz, Chem. Eng. J. 257 (2014) 98–104.
[8] Y. He, J.F. Gao, F.Q. Feng, C. Liu, Y.Z. Peng, S.Y. Wang, Chem. Eng. J. 179 (2012) 8–18.
[9] S. Nam, P.G. Tratnyek, Water Res. 34 (2000) 1837–1845.
[10] B. Yao, Y. Liu, D. Zou, Chemosphere 226 (2019) 298–306.
[11] C.E. Noradoun, I.F. Cheng, Environ. Sci. Technol. 39 (2005) 7158–7163.
[12] Y.H. Hsueh, P.H. Tsai, K.S. Lin, W.J. Ke, C.L. Chiang, J. Nanobiotechnol. 15 (2017) 77.
[13] Y. Mu, Z.H. Ai, L.Z. Zhang, Environ. Sci. Technol. 51 (2017) 8101–8109.
[14] N. Zhang, J. Chena, Z. Fang, E.P. Tsang, Chem. Eng. J. 369 (2019) 588–599.
[15] S.H. Joo, A.J. Feitz, T.D. Waite, Environ. Sci. Technol. 38 (2004) 2242–2247.
[16] C. Tan, Y. Dong, D. Fu, N. Gao, J. Ma, X. Liu, Chem. Eng. J. 334 (2018) 1006–1015.
[17] W. Chang, C.Y. Sun, X.B. Pang, H. Sheng, Y. Li, H.W. Ji, W.J. Song, C.C. Chen, W.H. Ma, J.C. Zhao, Angew. Chem. Int. Ed. 54 (2015) 2052–2056.
[18] C.Y. Sun, W. Chang, W.H. Ma, C.C. Chen, J.C. Zhao, Environ. Sci. Technol. 47 (2013) 2370–2377.
[19] G.D. Sheng, Y.Y. Shao, W.D. Ye, C.Y. Sun, C.C. Chen, J.C. Crittenden, C.L. Liu, ACS Sustain. Chem. Eng. 6 (2018) 6711–6717.
[20] S. Kang, S. Liu, H. Wang, W. Cai, J. Hazard. Mater. 307 (2016) 145–153.
[21] J. Farrell, N. Melitas, M. Kason, T. Li, Environ. Sci. Technol. 34 (2000) 2549–2556.
[22] X. Liu, Z. Cao, Z. Yuan, J. Zhang, X. Guo, Y. Yang, F. He, Y. Zhao, J. Xu, Chem. Eng. J. 334 (2018) 508–518.
[23] J.A. Donadelli, L. Carlos, A. Arques, F.S. García Einschlag, Appl. Catal. B 231 (2018) 51–61.
[24] Y.H. Huang, T.C. Zhang, Water Res. 39 (2005) 1751–1760.
[25] K.V.K. Ansaf, S. Ambika, I.M. Nambi, Water Res. 102 (2016) 436–444.
[26] A.L. Lazrus, G.L. Kok, S.N. Gitlin, J.A. Lind, S.E. McLaren, Anal. Chem. 57 (1985) 917–922.
[27] B.L. Cushing, V.L. Kolesnichenko, C.J. O'Connor, Chem. Rev. 104 (2004) 3893–3946.
[28] L. Lu, Z. Ai, J. Li, Z. Zheng, Q. Li, L. Zhang, Cryst. Growth Des. 7 (2017) 459–464.
[29] J. Xu, X. Wang, F. Pan, Y. Qin, J. Xia, J. Li, F. Wu, Chem. Eng. J. 353 (2018) 542–549.
[30] D.M. Cwiertny, A.L. Roberts, Environ. Sci. Technol. 39 (2005) 8948–8957.
[31] I.A. Katsoyiannis, T. Ruettimann, S.J. Hug, Environ. Sci. Technol. 42 (2008) 7424–7430.
[32] C. He, J. Yang, L.F. Zhu, Q. Zhang, W.C. Liao, S.K. Liu, Y. Liao, M.A. Asi, D. Shu, Sep. Purif. Technol. 117 (2013) 59–68.
[33] L. Santos-Juanes, F.S.G. Einschlag, A.M. Amat, A. Arques, Chem. Eng. J. 310 (2017) 484–490.
[34] F. Cattaruzza, D. Fiorani, A. Flamini, P. Imperatori, G. Scavia, L. Suber, A.M. Testa, Chem. Mater. 17 (2005) 3311–3316.
[35] S.S. Yang, P.X. Wu, J.Q. Liu, M.Q. Chen, Z. Ahmed, N.W. Zhu, Chem. Eng. J. 350 (2018) 484–495.
[36] Y.X. Wang, H.Q. Sun, X.G. Duan, H.M. Ang, M.O. Tadé, Appl. Catal. B 172 (2015) 73–81.
[37] J.E. Martin, A.A. Herzing, W. Yan, X.Q. Li, B.E. Koel, C.J. Kiely, W.X. Zhang, Langmuir 24 (2008) 4329–4334.
[38] L. Lu, Z. Ai, J. Li, Z. Zheng, Q. Li, L.Z. Zhang, Cryst. Growth Des. 7 (2007) 459–464.
[39] X.M. Zhou, J.Y. Lan, G. Liu, K. Deng, Y.L. Yang, G.J. Nie, J.G. Yu, L.J. Zhi, Angew. Chem. Int. Ed. 51 (2012) 178–182.
[40] P. Zhang, W. Huang, Z. Ji, C.G. Zhou, S.H. Yuan, Geochim. Cosmochim. Acta 238 (2018) 394–410.
[41] P.S. Rao, E. Hayon, J. Phys. Chem. 79 (1975) 397–402.
[42] R. Flyunt, O. Makogon, S. Naumov, C. Schöneich, K.D. Asmus, J. Phys. Chem. A 111 (2007) 11618–11625.
[43] M.H. Nie, C.X. Yan, X.Y. Xiong, X.M. Wen, X. Yang, Z.L. Lv, W.B. Dong, Chem. Eng. J. 348 (2018) 455–463.
[44] M.H. Nie, Y. Yang, Z.J. Zhang, C.X. Yan, X.N. Wang, H.J. Li, C.Y. Yan, X.N. Wang, H.J. Li, W.B. Dong, Chem. Eng. J. 246 (2014) 373–382.
[45] B. Sahoo, A.-E. Surkus, M.-M. Pohl, J. Radnik, M. Schneider, S. Bachmann, M. Scalone, K. Junge, M. Beller, Angew. Chem. Int. Ed. 56 (2017) 11242–11247.
[46] C. Sun, D. Zhao, C. Chen, W. Ma, J. Zhao, Environ. Sci. Technol. 43 (2009) 157–162.
[47] K. Biswas, S. Chattopadhyay, Y. Jing, R. Che, G. De, B. Basu, D. Zhao, Ind. Eng. Chem. Res. 58 (2019) 2159–2169.